CIRCUIT AND ELECTROMAGNETIC SYSTEM DESIGN NOTES

Note 35

12 February 1988

# OPTIMAL POSITIONING OF A SET OF PEAKER ARMS IN A GROUND PLANE

*D.V. Giri*

Pro-Tech, 125 University Avenue, Berkeley, California 94710

and

*Carl E. Baum*

Air Force Weapons Laboratory, Kirtland AFB, New Mexico 87117

## ABSTRACT

Marx type of pulse generators have been used to provide the transient energy to various types of EMP simulators such as the radiating, transmission line and the hybrid types. The components of the pulser viz., Marx column, peaking capacitor and the output switch may be configured in many different ways depending on the simulator type, high voltage considerations, etc. In a two-parallel plate transmission line type of simulator, one possible configuration is to distribute a set of peaker arms in the ground plane with the Marx column behind it and the output switch in the active propagation region. In this note, electromagnetically optimal positioning of a given number of peaker arms in the ground plane, is studied in detail.

## CONTENTS

## I. Introduction

When one thinks of an EMP pulser as a part of wave generating and launching system, one can appreciate the need for electromagnetic optimization of the manner in which the individual pulser components are configured. In other words, in the interest of improved simulation fidelity, it is imperative to choose high quality pulser components, and optimize their configuration in terms of physical, high voltage and electromagnetic considerations.

Consider for example, a cylindrical transmission line which is often used to simulate a free-space planar electromagnetic wave. The cylindrical transmission line formed by two parallel plates for instance, is typically matched by conical transmission lines on either side. The conical transmission lines work as a wave launcher on one side and a wave receptor for termination on the other side. Both vertical and horizontal polarizations shown schematically in figure 1, have been employed in practice. Figure 1a is the side view of a transmission line geometry for propagating a vertically polarized transient wave. Figures 1b and 1c show the side and top views of a transmission line geometry with a double conical launch. In either case, sources are connected between the line conductor and a ground plane. In the case of the horizontally polarized line, a wedge shaped ground plane may be introduced in the apex region of the wave launching conical transmission line so that two pulsers can be used in series [1 and 2].

With regards to the source of transient energy, Marx generators have been used in exciting such structures with fast rising pulses with rise times significantly shorter than the transit time across their cross sectional dimensions. Furthermore, in both geometries of figure 1, symmetry or image planes can be taken advantage of, in facilitating the configuration of pulser components, shielding the instrumentation, etc. The Marx pulsers, schematically shown as "sources" in figure 1, comprise several components which have to be configured in some optimal way. However, when a ground plane is available, it can be effectively used while interconnecting the individual pulser components. One may think of placing the Marx column behind the ground plane, the peaker arms distributed in the ground plane and the output switch will then be on the wave propagating side. The output switch, typically mono- or bi-conical in shape may

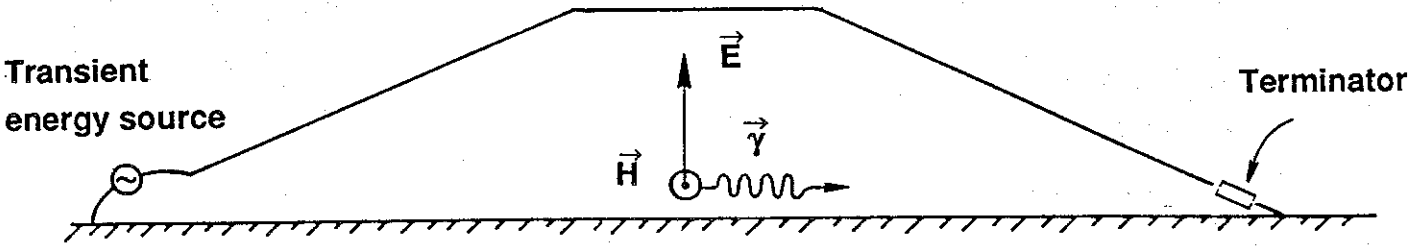


(a) Side view of a vertically polarized line with a flat image plane.

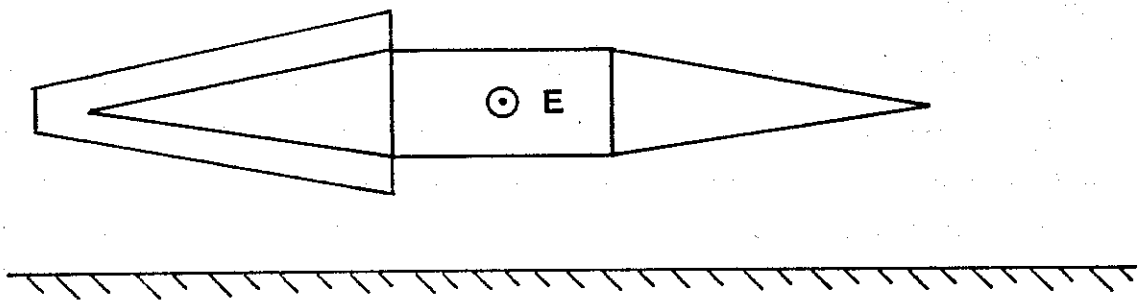


(b) Side view of a horizontally polarized line supported above ground.

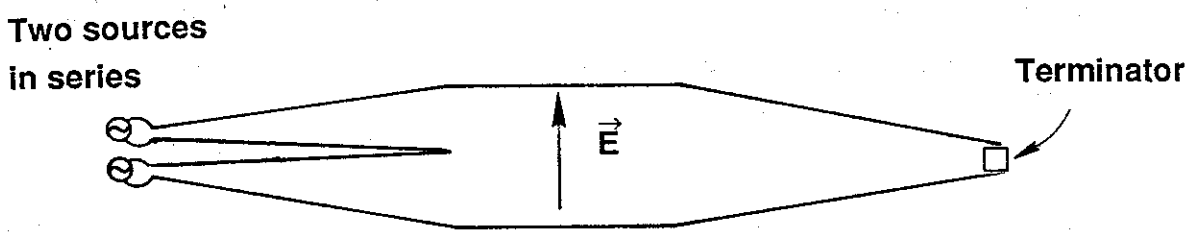


(c) Top view of case (b) above with a double conical launch and a single conical wave receptor.

Figure 1. Examples of transmission line geometries useful in simulating a free space planar electromagnetic wave.

smoothly transition to the top plate of the wave launcher.

In the context of the pulser configuration outlined above, one recognizes an electromagnetic problem of finding the optimal peaker arm distribution in the ground plane. This is the problem that has been addressed in this note. It is desirable to have equal currents flowing in all of the peakers, during both the charge cycle and the discharge cycle (after the closure of the output switch). The requirement of equi-peaker arm currents is relatively more important during the discharge cycle (with comparatively fast times and high frequencies) when the return currents are flowing in the ground plane. This is the essence of electromagnetic optimization of the peaker arm distributions in the ground plane. Of course, once the peaker arm distribution is optimized for the discharge cycle, the positioning and orientation of the Marx column in addition to a careful design of the interconnections can ensure equal peaker arm currents in the charge cycle as well.

With reference to figure 2a, let us define a boundary value problem which approximates the real problem. Consider an equivalent line current or line charge oriented so that it makes an angle $\theta_0$ with respect to a perfectly conducting, infinite ground plane. This line source is placed along the center line of a conical (triangular) plate so as to give approximately the same potential and field distribution as the conical plate "far" from the plate (in a spherical angular sense). Provided the conical plate is narrow in angle compared to the angle $\theta_o$ from the ground plane, this should be a good approximation. Imagine a circular perforation in the ground plane centered at the point of intersection of the line source and the ground plane. Equivalently, this point would be the theoretical apex of the conical-wave-launch transmission line. The excitation current $I$ (amps) flows out on the line source and returns to the apex via the terminator at the far end and the ground plane. The problem is one of distributing a given number $N_p$ of peaker arms (treated as conductors) in the circular hole, in such a manner that all of the peaker arms carry equal currents. Such a distribution is schematically shown in figure 2b.

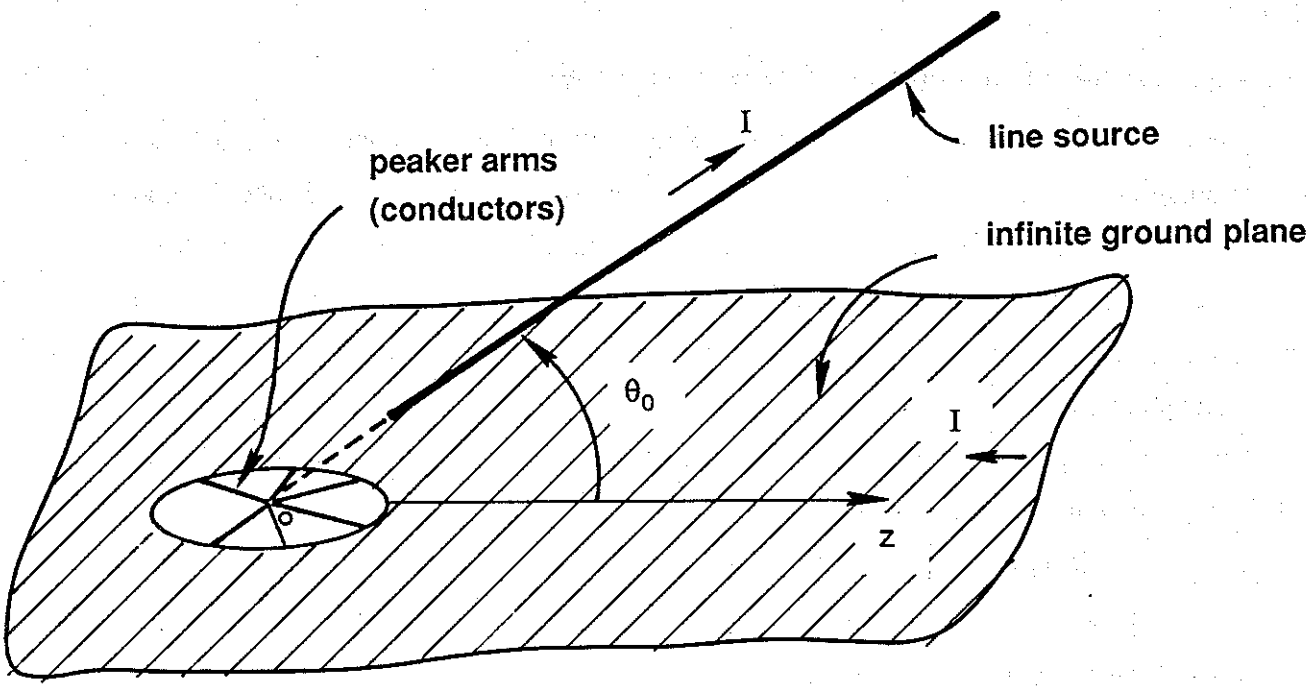


(a) Sloping line current/charge source.

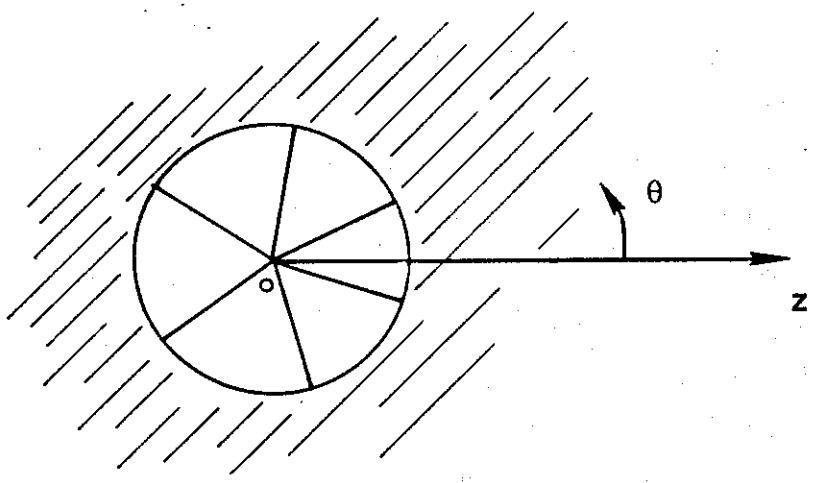


(b) Peaker arms distribution in the ground plane.

Figure 2. Defining the problem of determining the optimal peaker arm distribution in the ground plane.

The electromagnetic problem outlined in the preceding paragraph is in sharp contrast with an earlier problem addressed by the authors [3], wherein the optimal peaker arm locations were determined for the case of Marx column above the ground plane and the peaker arms surrounding it.

Returning to the problem at hand, the method used here consists of formulating the complex potential and field in both spherical and equivalent cylindrical coordinates [4 and 5]. The real ($u$) and imaginary (v) parts of the complex potential ($w$) correspond to the electric potential (volts) and magnetic potential (amps) respectively. The optimal peaker arm locations are derivable by studying the distribution of the magnetic potential in the ground plane and requiring equal $\Delta$v ($=2\pi/N_p$) between adjacent peaker arms. In other words, we study the magnetic field lines on the ground plane and place the conductors, i.e., peaker arms so that they carry equal currents. After the required calculations are performed for optimal peaker arm locations, some practical considerations such as use of "teeth"-like metallic interconnections between the peaker arms and the ground plane, raising the peaker arms slightly up above the ground plane, are also discussed.

## II. Complex Potential and Complex Field

Consider a conical transmission line formed by two triangular shaped plates as indicated in figure 3. A set of rectangular $(x, y, z)$ and spherical $(r, \theta, \phi)$ coordinate systems with their coincident origins at the transmission line apex O is also indicated in the figure. It is well known that such a structure supports a spherical TEM wave propagating along the radial direction [4, 5, 6 and 7]. The complex potential may be written after removing the $r$ dependence $(exp\ (-\gamma r)/r)$ as,

$$w\ (\theta, \phi) = [u\ (\theta, \phi) + j\,\mathrm{v}\ (\theta, \phi)\,] \tag{1}$$

where $u$ and v satisfy the two-dimensional Laplace equation on a spherical surface

$$sin\ (\theta)\frac{\partial}{\partial\theta}\left[\ sin\ (\theta)\frac{\partial}{\partial\theta}\begin{bmatrix} u(\theta,\phi) \\ \mathrm{v}(\theta,\phi)\end{bmatrix}\ \right] + \frac{\partial^2}{\partial\phi^2}\begin{bmatrix} u(\theta,\phi) \\ \mathrm{v}(\theta,\phi)\end{bmatrix} = 0 \tag{2}$$

and $\gamma$ is the propagation constant. Smythe [4] has also shown that $u + j\mathrm{v}$ is of the form

$$u\ (\theta, \phi) + j\,\mathrm{v}\ (\theta, \phi) = f_1\,(2\,e^{j\phi}\,tan\,(\theta/2)\,) \tag{3}$$

The above form of the TEM solution leads to an equivalent cylindrical transmission line via a coordinate transformation. This transformation from the spherical $(r, \theta, \phi)$ to an equivalent cylindrical $(\psi', \phi, z')$ is of the form

$$\begin{aligned} \psi' &= 2\,z_o\ tan\ (\theta/2) \\ \phi &= \phi \\ z' &= r \end{aligned} \tag{4}$$

where $z_o$ is a constant to be used later. Note that the $\phi$ coordinate remains unchanged and the $\theta$ coordinate maps only to the $\psi'$ (cylindrical radius) coordinate. Furthermore, $(x', y', z')$ is a rectangular coordinate system associated with the cylindrical transmission line. Smythe's [4] development of an equivalent cylindrical transmission line has been used [6 and 7] in solving for the impedance and field distribution of the TEM wave in a conical transmission line. The method used in solving the equivalent cylindrical transmission line is the familiar conformal mapping method.

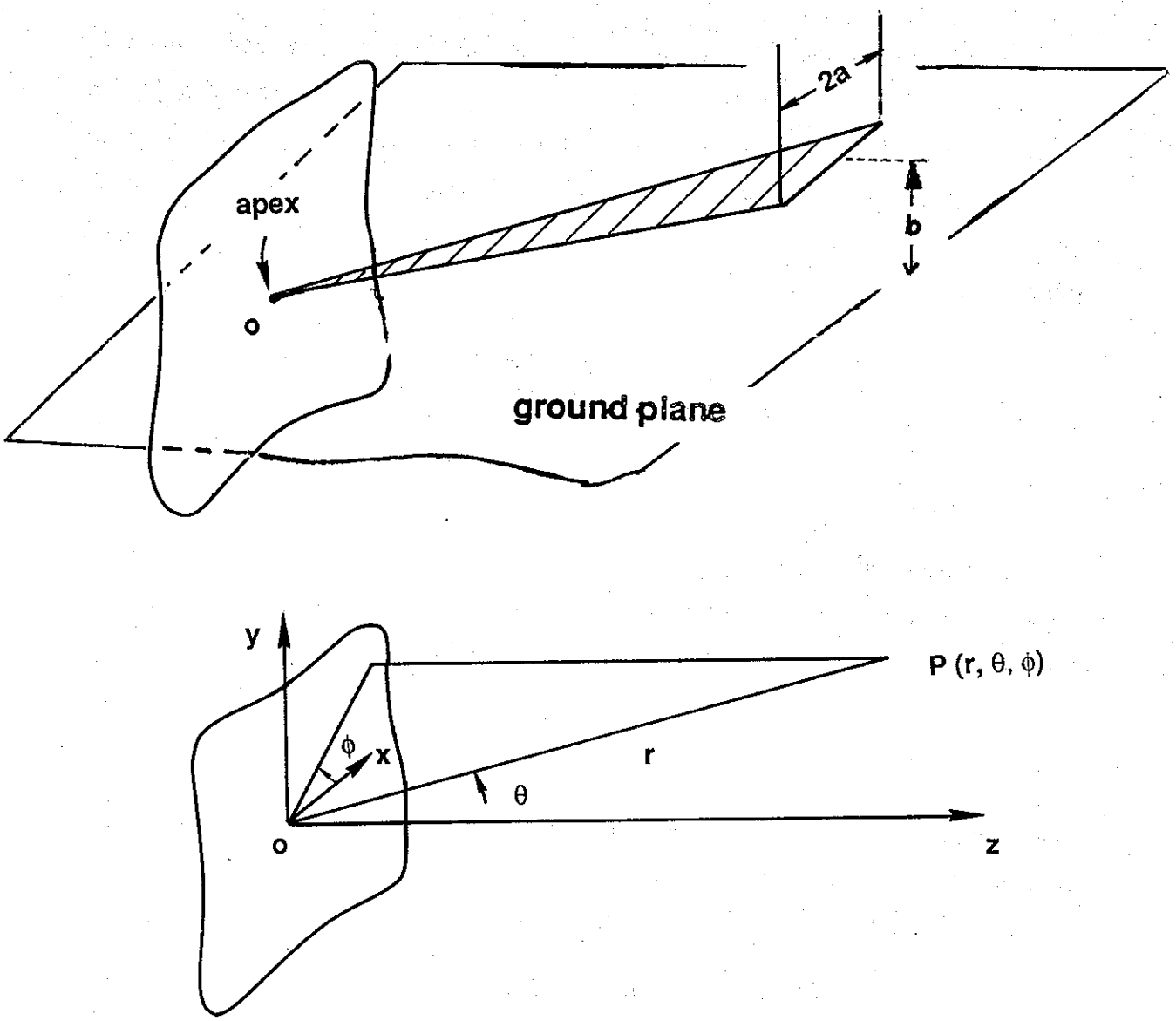


Figure 3. Conical transmission line with rectangular (x, y, z) and spherical (r, θ, ϕ) coordinate systems.

The procedure of going from a conical transmission line to an equivalent cylindrical transmission line can also be interpreted in terms of a stereographic projection [7]. In this projection (figure 4), a point $(x, y, l)$ in the $z = l$ plane is first radially projected onto a point $(x'', y'', z'')$ on a sphere of radius $l$ and then stereographically on to $(x', y', l)$. A planar view of the stereographic projection is shown in figure 5 and the equivalent cylindrical transmission line in figure 6. The projection results in

$$\begin{aligned} x' &= \frac{2\,x\,l}{l+\sqrt{l^2+x^2+y^2}} \\ y' &= \frac{2\,y\,l}{l+\sqrt{l^2+x^2+y^2}} \end{aligned} \tag{5}$$

The cylindrical transmission line consists of two plates of circular arc (see figure 6), in the $z'$ plane, and the TEM solution for such a line is easily obtained via conformal transformation [7]. Also, in terms of the spherical coordinates, (5) may be written as

$$\begin{aligned} x' &= 2\,l\ tan\ (\theta/2)\ cos\ (\phi) \\ y' &= 2\,l\ tan\ (\theta/2)\ sin\ (\phi) \end{aligned} \tag{6}$$

The transformation equations that take one from the $z'$ plane to the complex potential $w$ plane involves elliptic integrals and functions [7] and is not repeated here. The electric and magnetic fields may now be summarized as follows

$$\begin{aligned} \vec{E}\,(\vec{r}\,) &= \vec{E}\,(r, \theta, \phi) = \vec{V}_s\,(\theta, \phi)\ exp\ (-\gamma r)\,/r \\ \vec{H}\,(\vec{r}\,) &= \vec{1}_r \times \vec{E}\,(\vec{r}\,)\,/\,Z_o \end{aligned} \tag{7}$$

where $Z_o$ is the intrinsic impedance of the medium in which the plates are immersed. $\vec{V}_s\,(\theta, \phi)$ is a voltage distribution function on a spherical surface and is obtained from the gradient of the complex potential as,

$$\vec{V}_s\,(\theta, \phi) = -\frac{\partial v}{\partial \theta}\,\vec{1}_\theta - csc\ (\theta)\,\frac{\partial v}{\partial \theta}\,\vec{1}_\phi \tag{8}$$

where v is the imaginary part of the complex potential function $w\,(z')$ (*known*). The fields

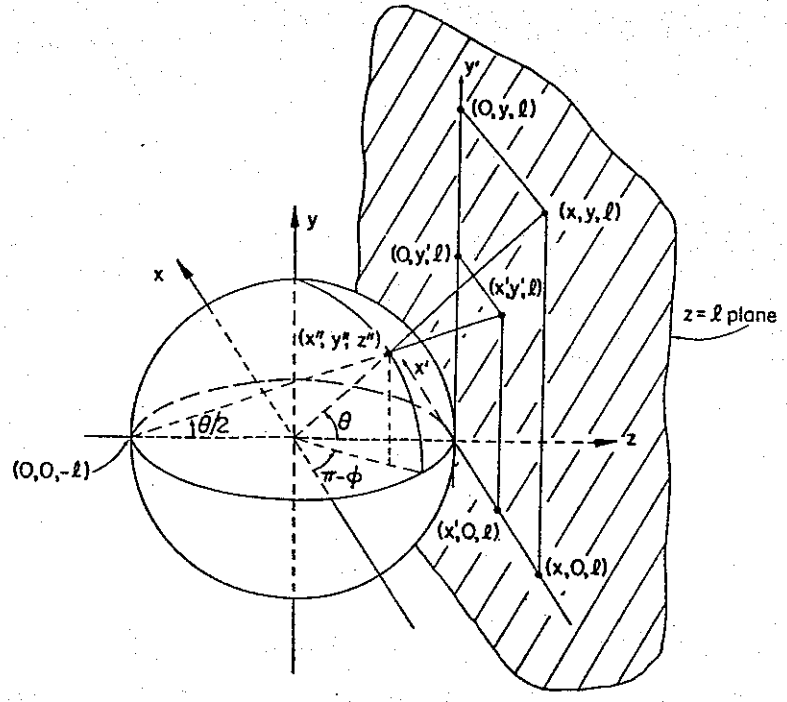


**Figure 4. Stereographic projection procedure.**

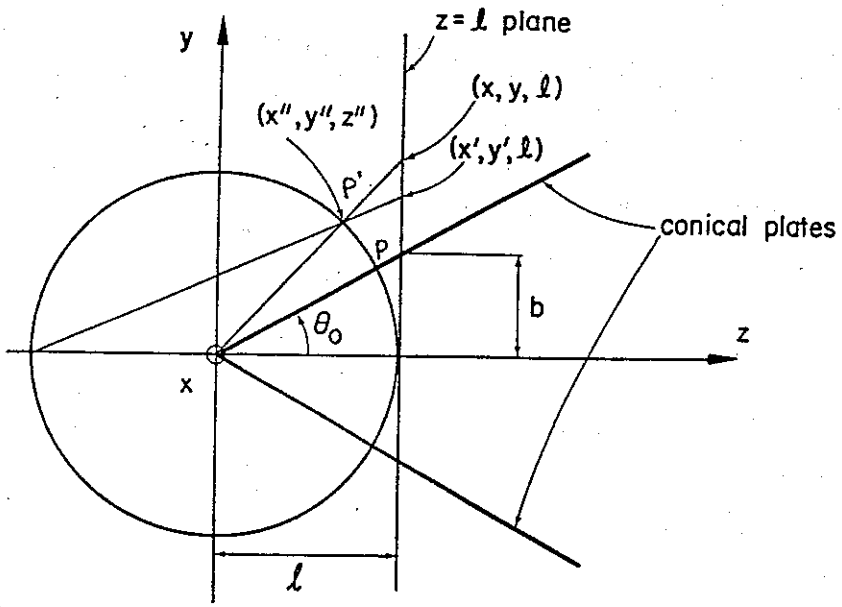


**Figure 5. Planar view of stereographic projection.**

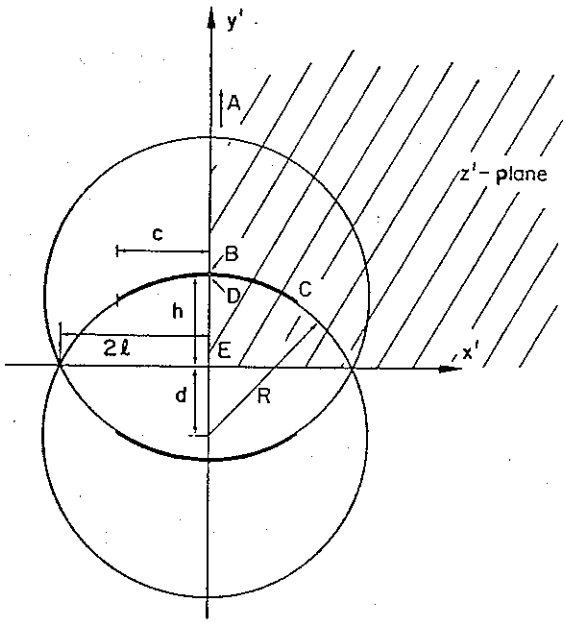


$R = (2\ell/b)\sqrt{b^2+\ell^2}$

$d = 2\ell^2/b$

$h = R - d$

$c = 2a\ell/(\sqrt{a^2+b^2+\ell^2}+\ell)$

**Figure 6. Equivalent cylindrical transmission line.**

**Note: All the figures on this page are reporduced from [7].**

may be written in various coordinate systems as follows.

$$\text{Complex field} \equiv \frac{-\partial w(z')}{\partial z'}$$

$$= \left[ E'_y(x', y', l) + j\, E'_x(x', y', l) \right]$$

$$= \left[ -H'_x(x', y', l) + j\, H'_y(x', y', l) \right] \tag{9}$$

Since $w(z')$ is a known function, $E'_x$ and $E'_y$ or $\vec{E}'(x', y', l)$ is computable. Recall that $(x' + jy')$ is the complex plane corresponding to the cylindrical transmission line formed by two curved plates (see figure 6). Knowing $\vec{E}'(x', y', l)$, $\vec{E}(r, \theta, \phi)$ and $\vec{E}(x, y\ l)$ can be written down via the coordinate transformations as follows.

$$E_r(r, \theta, \phi) = 0$$

$$E_\theta(r,\theta,\phi) = l\ sec^2\left(\frac{\theta}{2}\right)\left[ cos(\phi)E'_x(x', y', l) + sin(\phi)E'_y(x', y', l) \right] \frac{e^{(-\gamma r)}}{r} \tag{10}$$

$$E_\phi(r,\theta,\phi) = l\ sec^2\left(\frac{\theta}{2}\right)\left[ -sin(\phi)E'_x(x', y', l) + cos(\phi)E'_y(x', y', l) \right] \frac{e^{(-\gamma r)}}{r}$$

and

$$E_x(x, y, l) = l\ sec^2\left(\frac{\theta}{2}\right) \frac{e^{-(\gamma r)}}{r}\Big[ \{cos(\theta)cos^2(\phi) + sin^2(\phi)\}E'_x(x', y', l)$$

$$+ \{cos(\phi)sin(\phi)(cos(\theta) - 1)\}E'_y(x', y', l) \Big]$$

$$E_y(x, y, l) = l\ sec^2\left(\frac{\theta}{2}\right) \frac{e^{-(\gamma r)}}{r}\Big[ \{cos(\phi)sin(\phi)(cos(\theta) - 1)\}E'_x(x', y', l) \tag{11}$$

$$+ \{cos(\theta)sin^2(\phi) + cos^2(\phi)\}E'_y(x', y', l) \Big]$$

$$E_z(x, y, l) = l\ sec^2\left(\frac{\theta}{2}\right) \frac{e^{-(\gamma r)}}{r}\Big[ -sin(\theta)cos(\phi)E'_x(x', y', l) - sin(\theta)sin(\phi)E'_y(x', y', l) \Big]$$

where

$$\begin{aligned} r &= (x^2+y^2+z^2)^{1/2} \\ \theta &= \arccos(z/r) \\ \phi &= \arctan(y/x) \end{aligned} \tag{12}$$

This formally completes a review of complex potentials and fields in spherical (natural coordinate system for the conical line), equivalent cylindrical and rectangular (practical, in terms of measurement) coordinate system.

In the next section, we briefly review the TEM solution of a two-wire cylindrical line and apply the results of this and the next section to the problem at hand.

## III. Two-Wire Cylindrical Transmission Line

In the previous section, we reviewed how the complex potentials and electromagnetic fields can be obtained for the problem of a conical transmission line. The method uses a combination of stereographic projection and conformal transformation. It can now be observed that for a narrow conical transmission line resulting in a high characteristic TEM mode impedance, the plates of the line may be replaced by line charges, to a first order approximation. A narrow or a high impedance line corresponds to one with the plate width (2a) small compared to the plate separation (2b) in figure 3. With such an approximation in mind, we now briefly review the results of a two-wire line for later use.

A symmetrical two wire transmission line is a classical problem for which the TEM solution is well known and documented e.g., [8 and 9]. Figure 7 shows a symmetrical two-wire line made up of two cylindrical conductors each of radius $c_o$ and with a separation between their centers being 2b, in the $y$ direction. For convenience in the analysis, the coordinates are normalized by dividing by $b_o$, where $2b_o$ is the separation between infinitesimal line currents/charges from which the TEM solution is developed, so that referring to figures 7 and 8, we have

$$\begin{aligned} x_{norm} &= (x/b_o) \qquad y_{norm} = (y/b_o) \\ b' &= (b/b_o) \qquad c' = (c_o/b_o) \end{aligned} \tag{13}$$

One could think of the physical plane of cross section as a complex plane as given by

$$z_{norm} = x_{norm} + j\ y_{norm} \tag{14}$$

and the conformal mapping is given by

$$w_1(z_{norm}) = ln\left[\frac{z_{norm}+j}{z_{norm}-j}\right] = u_1 + j\ v_1 \tag{15}$$

expanding the above equation, we have

$$x_{norm} = \frac{sin\ (v_1)}{cosh\ (u_1) - cos\ (v_1)} \quad ; \quad y_{norm} = \frac{sinh\ (u_1)}{cosh\ (u_1) - cos\ (v_1)} \tag{16}$$

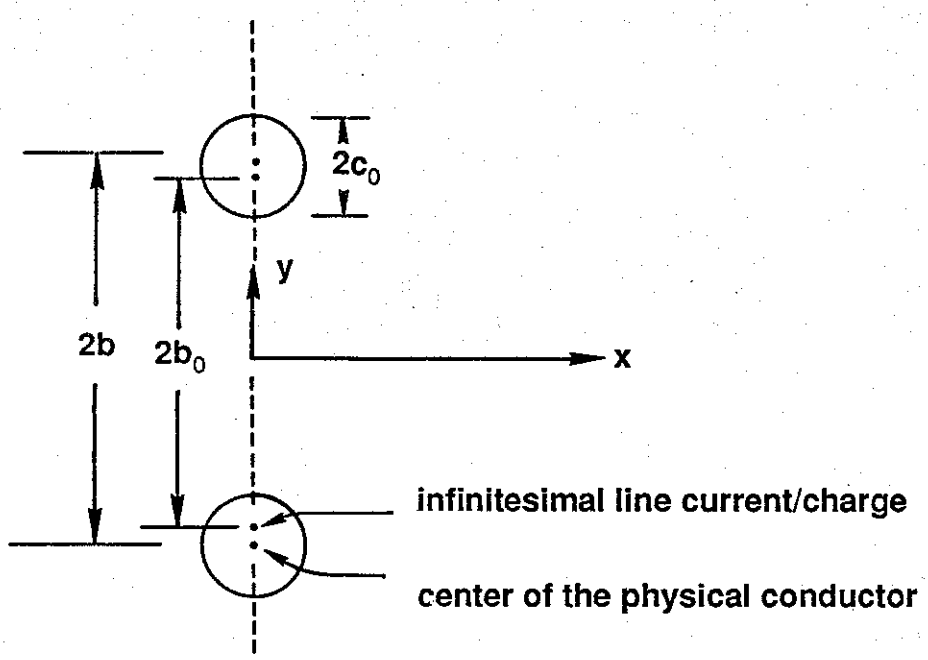


Figure 7. Symmetrical two wire transmission line (unnormalized coordinates).

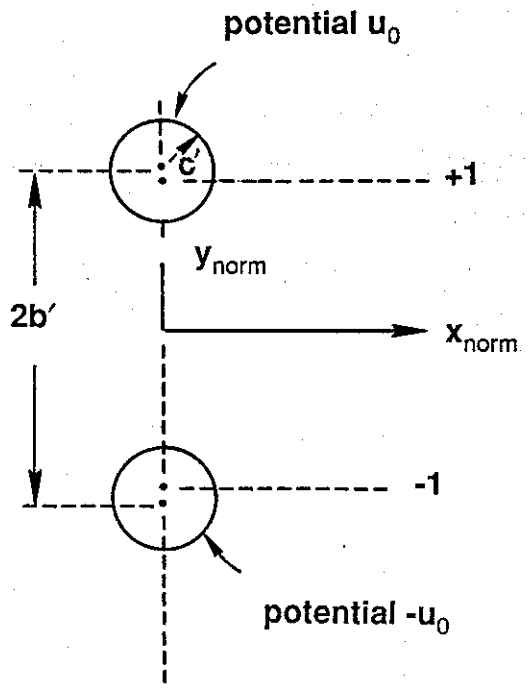


Figure 8. Symmetrical two wire transmission line (normalized coordinates).

and

$$u_1 = \frac{1}{2} ln \left[ \frac{x_{norm}^2 + (1+y_{norm})^2}{x_{norm}^2 + (1-y_{norm})^2} \right]$$

$$v_1 = arctan \left[ \frac{2x_{norm}}{x_{norm}^2 + y_{norm}^2 - 1} \right] \tag{17}$$

Equation (17) above is useful in computing the real and imaginary parts of the complex potential for a symmetrical two-wire line. The next step is to apply these results to the case of a conical transmission line that has been stereographically projected to a cylindrical transmission line. We are of course interested in the conical transmission line made up of two plates of zero width, in essence a conical transmission line of two line currents/charges.

We may now specialize the results of Section II to a case of a conical transmission line where the conductors have zero cross section. Specifically, figure 5 showed a planar view of the stereographic projection. A general point $P'(x'', y'', z'')$ in this figure was projected on to $(x', y', l)$ and $(x, y, l)$ planes. By moving the general point $P'(x'', y'', z'')$ to a point $P$ on the line current (i.e., plate of zero thickness or $a = 0$), we may redraw figures 5 and 6 as figures 9 and 10 for this special case. We still have,

$$x' = \frac{2xl}{l + \sqrt{x^2 + y^2 + l^2}} \quad ; \quad y' = \frac{2yl}{l + \sqrt{x^2 + y^2 + l^2}} \tag{18}$$

We recognize from figure 10 that the corresponding equivalent cylindrical line is made up of two infinitesimal wires, as opposed to curved plates. The separation between the "line currents" is $2h$ with $h$ given by

$$h = y' \text{ (when } y = b,\ x = 0, \text{ and } z = l)$$

$$= 2l \left[ \frac{b}{l + \sqrt{b^2 + l^2}} \right] \tag{19}$$

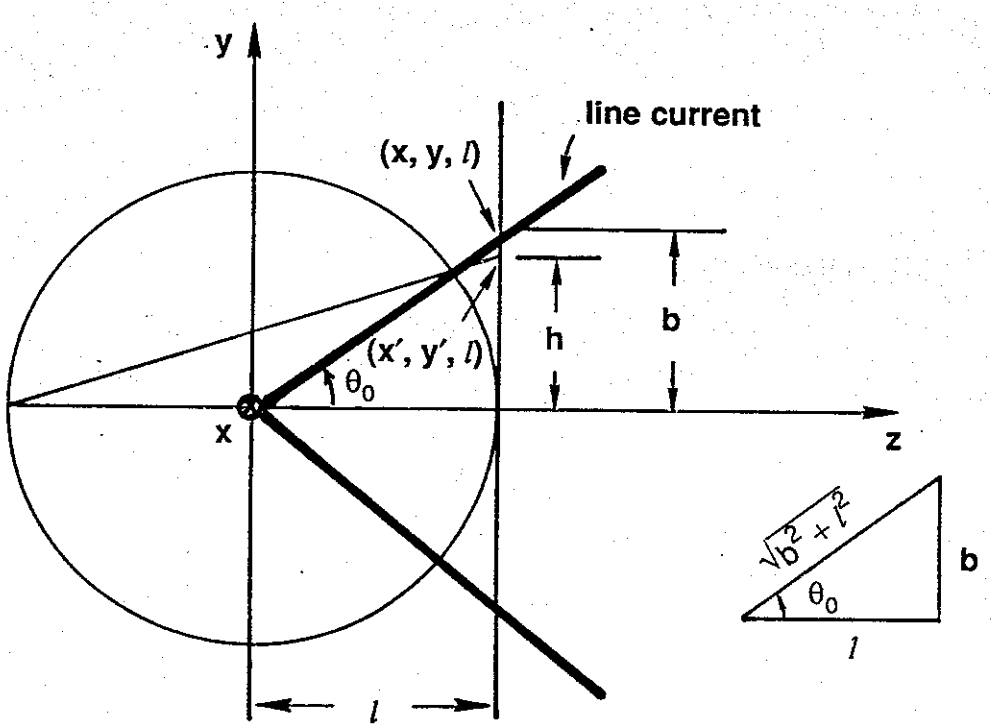


Figure 9. Planar view of the stereographic projection for the specialized conical transmission line of zero width plates.

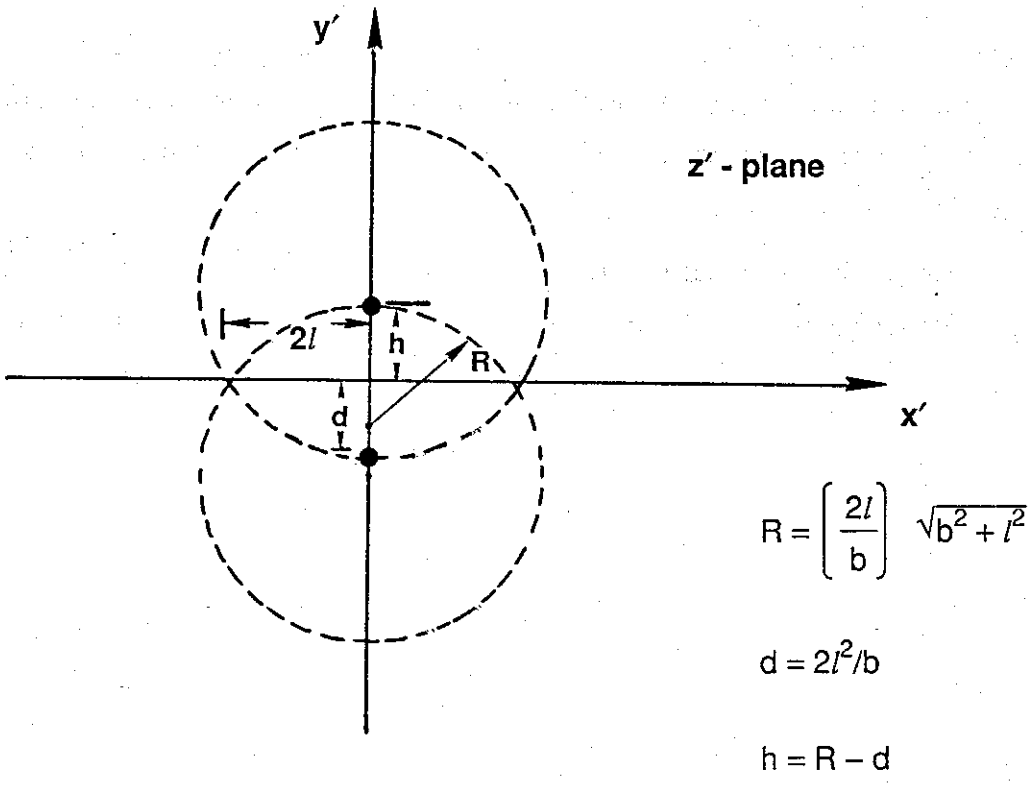


Figure 10. Equivalent cylindrical transmission line.

Also observe that

$$tan\ (\theta_o/2) = \frac{sin\ (\theta_o)}{1+cos\ (\theta_o)}$$

$$= \frac{b}{\sqrt{b^2+l^2}} \left[ \frac{1}{1+\frac{l}{\sqrt{b^2+l^2}}} \right]$$

$$= \frac{b}{l+\sqrt{b^2+l^2}} \tag{20}$$

Using (20) in (19) we have

$$h = 2l\ tan\ (\theta_o/2) \tag{21}$$

So, the conical transmission line formed by two line currents (see figure 2a) is thus equivalent to a cylindrical transmission line formed by two infinitesimal wires separated by a distance $2h$ where $h$ is given above, keeping in mind the cross section under consideration is given by $z = l$.

Now, for a symmetrical two-conductor transmission line, we have the complex potential given by (17). Specifically, the imaginary part $v_1(x', y')$ is given by

$$v_1(x', y') = arctan \left[ \frac{2x'_{norm}}{x'^2_{norm} + y'^2_{norm} - 1} \right] \tag{22}$$

with $x'_{norm} = (x'/h)$ and $y'_{norm} = (y'/h)$. On the ground or image plane $(y' = o)$,

$$v_1(x', o) = arctan \left[ \frac{2\,(x'/h)}{\left(\frac{x'}{h}\right)^2 - 1} \right]$$

$$= -arctan \left[ \frac{2\,(x'/h)}{1-(x'/h)^2} \right] = -2\ arctan\ (x'/h) \tag{23}$$

resulting in

$$x' = -h \tan\left[\frac{v_1(x', o)}{2}\right]$$

However, recall that

$$x' = 2l \tan(\theta/2) \cos(\phi) \tag{24}$$

describes the relationship with the spherical coordinates. On the ground or image plane $\phi = o$ or $\pi$, we therefore have,

$$\pm 2l \tan(\theta/2) = -h \tan\left[\frac{v_1(x', o)}{2}\right]$$

or

$$\tan(\theta/2) = \frac{h}{2l} \tan\left[\frac{v_1(x', o)}{2}\right] \tag{25}$$

We have chosen the negative sign on the left side above. The choice is not crucial since the optimal peaker location eventually is symmetric w.r.t. the $z$ axis. Using (21) in (25), we get

$$\tan(\theta/2) = \tan(\theta_o/2) \tan\left[\frac{v_1(x', o)}{2}\right] \tag{26}$$

The above equation is useful in determining the optimal peaker locations in the ground plane. This forms the subject of the following section.

## IV. Optimal Peaker Arm Locations in the Ground Plane

Having reviewed the procedure for determining the equivalent cylindrical transmission line for a given conical line and applied it to the problem at hand, we are now equipped to evaluate the peaker arm locations that are electromagnetically optimal. Recall the geometry of the problem depicted in figure 2. Let us say the number of peaker arms to be distributed in the ground plane is $N_p$. These $N_p$ peaker arms, which are regarded here as cylindrical conductors have to be distributed in such a way that they carry equal currents ($=I_p = I/N_p$) where $I$ is the total current (amps) flowing out on the line and returning in the ground plane (see figure 2a). The manner in which the peaker arms are distributed in the ground plane is schematically shown in figure 2b. The azimuthal angle $\theta_i$, measured anti-clockwise from the $+z$ axis, determines the location of each of the $N_p$ peakers for $i = 1, 2, 3.....N_p$. It is observed that one way of accounting for the symmetry about the $z$ axis is as follows.

$$\left.\begin{aligned} &\theta_1 = 0 \\ &\theta_i = -\theta_{N_p-(i-2)} \\ &\text{for } i = 2, 3..... (N_p+1)/2 \end{aligned}\right\} \quad \text{for } N_p \text{ odd} \tag{27}$$

and

$$\left.\begin{aligned} &\theta_i = -\theta_{N_p-(i-1)} \\ &\text{for } i = 1, 2,..... N_p/2 \end{aligned}\right\} \quad \text{for } N_p \text{ even} \tag{28}$$

The notational details of peaker distributions in the ground plane for both cases of $N_p$ *odd* (example of 5) and $N_p$ *even* (example of 6) are shown i figures 11 and 12.

Next, we turn our attention to the determination of locations in the ground plane of a given number ($N_p$) of peaker arms. Recall that we had earlier derived the following result (see (25))

$$\tan(\theta/2) = \tan(\theta_o/2)\ \tan\left[\frac{v_1(x', o)}{2}\right] \tag{29}$$

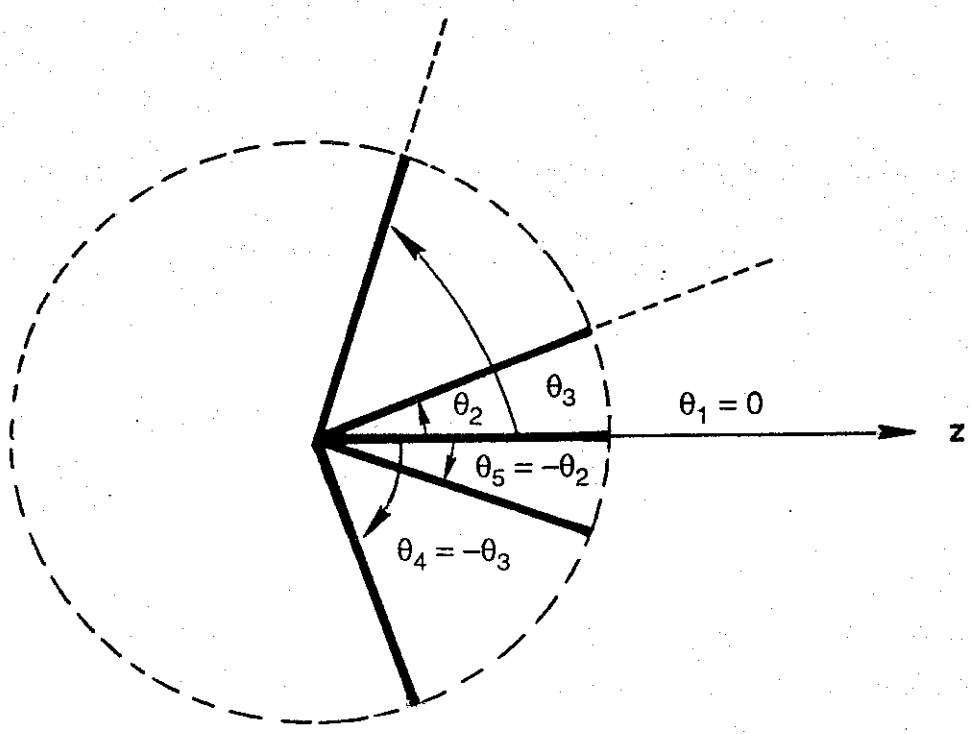


**Figure 11.** **Notation for odd number of peakers (Example $N_p = 5$) $N_p$ = odd, $\theta_1 = 0$; $\theta_i = -\theta_{N_{p-(i-2)}}$ for $i = 2, 3$ ..... $(N_p+1)/2$. (Prefered distribution.)**

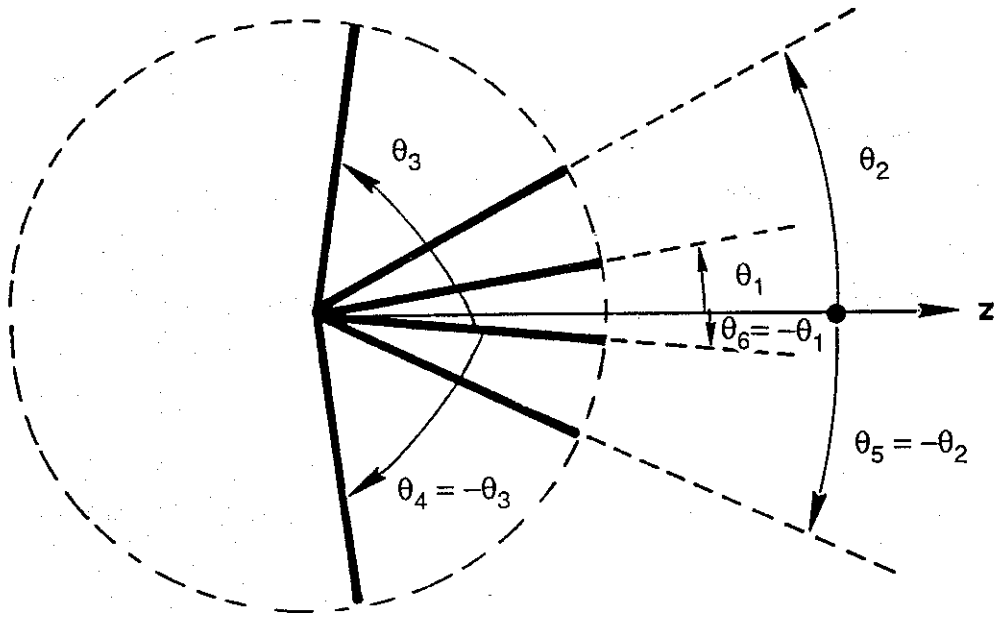


**Figure 12.** **Notation for even number of peakers (Example $N_p = 6$) $N_p$ = even; $\theta_i = \theta_{N_{p-(i-1)}}$ for $i = 1, 2,$ .....$N_p/2$. (Preferred distribution.)**

Consequently, if we had $N_p$ number of peaker arms, they may be chosen according as

$$tan\ (\theta_i/2) = tan\ (\theta_o/2)\ tan\ (v_i/2) \tag{30}$$

with

$$\left.\begin{aligned} v_i &= v_1 + (i-1)\ \Delta v \quad ;\quad i = 1, 2....N_p \\ v_1 &= (0\pi) \text{ for } N_p \text{ odd} \\ v_1 &= (\pi/N_p) \text{ for } N_p \text{ even} \end{aligned}\right\} \tag{31}$$

Observe that if $\Delta v$ between adjacent peakers is held constant, it is the same as having equal currents in each peaker. There is a $2\pi$ change in $v$, as one goes around from $\theta = 0$ to $\theta = 2\pi$, resulting in a choice of

$$\Delta v = (2\pi/N_p) \tag{32}$$

Equation (30) can be rewritten as

$$\theta_i = 2\ arctan\left[tan\left(\frac{\theta_o}{2}\right)\ tan\left(\frac{v_i}{2}\right)\right] \tag{33}$$

which can now be used along with (31) and (32), in computing the peaker locations in the ground plane.

In concluding this section, we also observe that there exists yet another way albeit less preferred way, of distributing odd or even number of peaker arms and still preserve the symmetry about the $z$ axis. Recall that for $N_p$ *odd*, we chose to place one peaker arm on the $+z$ axis and no peaker arms on the + or $-z$ axis for the case of $N_p$ *even*. The alternate possibility is to place one peaker arm on the $-z$ axis for $N_p$ *odd* and, one peaker arm each on the $+z$ and $-z$ axis for the case of $N_p$ *even*. This alternate possibility still preserves the symmetry about the $z$ axis and is governed by the following equations

$$\theta_i = 2\ arctan\left[tan\left(\frac{\theta_o}{2}\right)\ tan\left(\frac{v_i}{2}\right)\right] \tag{34}$$

with

$$v_i = v_1 + (i-1)\,\Delta v \quad ; \quad i = 1, 2.....N_p \tag{35}$$

$$\Delta v = 2\pi/N_p \tag{36}$$

as before. The change is in the initial value $v_1$ given by

$$\begin{aligned} v_1 &= \pi \qquad \text{for} \quad N_p \ \textit{odd} \\ v_1 &= (0\,\pi) \quad \text{for} \quad N_p \ \textit{even} \end{aligned} \tag{37}$$

It is easily verified that the above choice results in a single peaker arm on the $-z$ axis for $N_p$ *odd* corresponding to $v_1 = \pi$. The peaker arms are counted anti-clockwise starting with the one on the $-z$ axis as the first one. Similarly for the case of $N_p$ *even*, the first peaker ($i = 1$) is on the $+z$ axis and the $i = \left[\frac{N_p}{2} + 1\right]$ peaker will lie on the $-z$ axis.

The above outlined alternate choices of peaker arm distributions are illustrated in figures 13 and 14. These choices always place a peaker arm on the $-z$ axis. Since most of the return current is flowing from the forward direction (near $\theta = 0$), the distribution of figures 11 and 12 is preferred in comparison with those in figures 13 and 14. The alternate choice illustrated in figures 13 and 14 is not pursued any further.

In the next section, we present illustrative examples of peaker arm distributions for various launch angles and varying number of peaker arms, for each angle of launch.

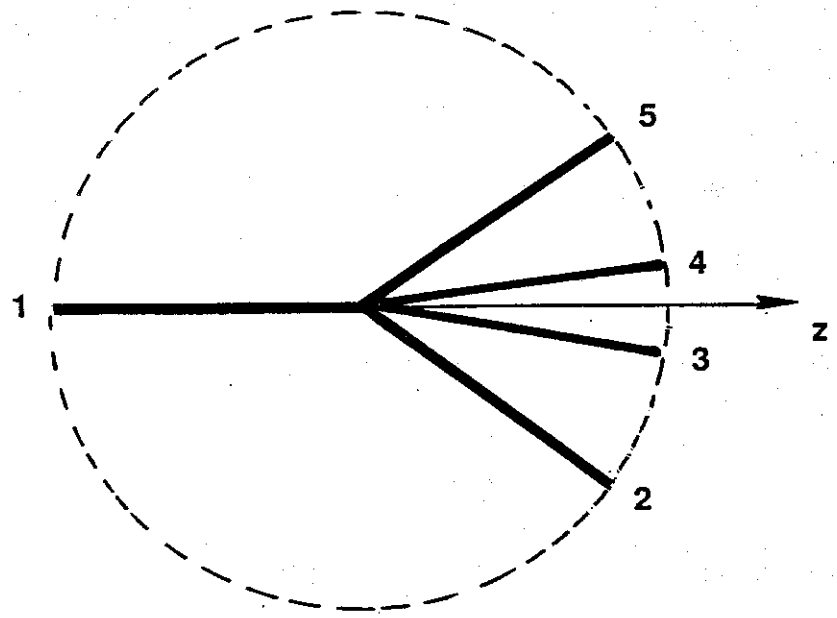


**Figure 13.** **An alternate distribution (less prefered) of peaker arms for the case of $N_p$ odd (Example $N_p = 5$) (see figure 11 for comparison).**

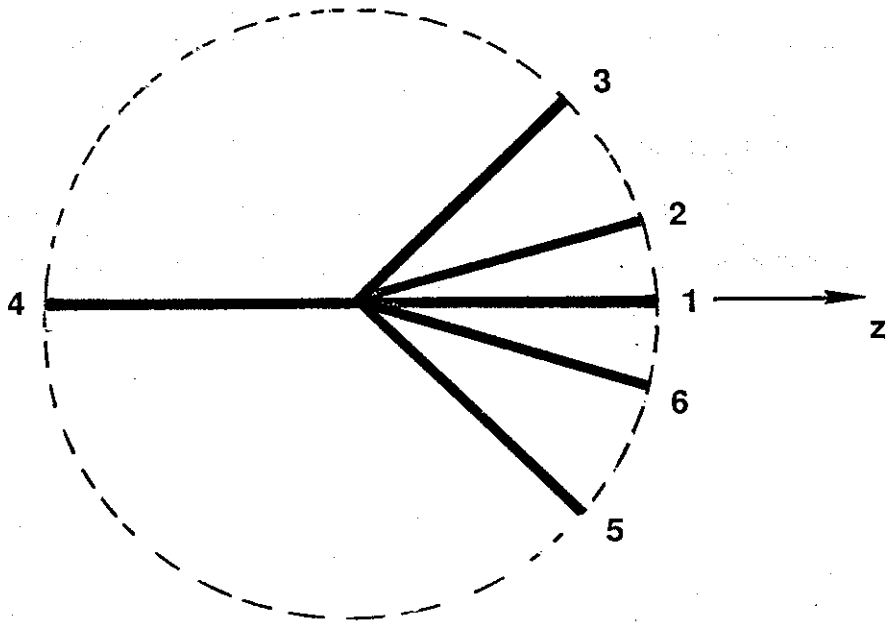


**Figure 14.** **An alternate distribution (less prefered) of peaker arms for the case of $N_p$ even (Example $N_p = 6$) (see figure 12 for comparison).**

## V. Illustrative Numerical Examples

In this section, we present illustrative examples for peaker arm locations in the ground plane. Let us consider five values of $\theta_o$, the angle between the top plate and the ground plane in the input wave launching section. These five values of $\theta_o$ are 10°, 15°, 20°, 25° and 30°. Of course, calculations such as the ones illustrated here, should be repeated for particular wave launchers existing or planned. For each value of $\theta_o$, 10 different values of $N_p$, the number of peaker arms ranging from $N_p = 1$ to 10 are considered. The equations, derived earlier, that are useful in determining the peaker locations are reproduced below.

$$\left.\begin{aligned} \theta_i &= 2\, arctan\left[ tan\left(\frac{\theta_o}{2}\right)\ tan\left(\frac{v_i}{2}\right)\right] \\ v_i &= v_1 + (i-1)\,\Delta v \\ \Delta v &= 2\pi/N_p \\ i &= 1, 2, .....N_p \end{aligned}\right\} \qquad (38)$$

The symmetry about the $+z$ axis, simplifies the computations according as (27) and (28) for $N_p$ *odd* and *even* respectively. The choice of $v_1$ is given in (31) and it determines the location of the first peaker arm. Once again, the symmetry of peaker arm locations about the $+z$ axis is useful in making this choice of $v_1$, tabulated in table 1. It is assumed that all peaker arms are of the same length and the numerical results presented in this section indicate the positions of the peaker arms in a circular hole cut out in the ground plane. These positions are optimal in the sense that all the peakers carry nearly the same current in the event of return current flowing in the ground plane.

The above equation (38) along with $v_1$ listed in table 1 are used in performing all the required numerical computations. Note that the choice of $v_1$ is such that for the case of $N_p$ *odd*, one has a peaker arm on the $+z$ axis and for the case of $N_p$ *even*, there are no peaker arms on the $z$ axis. This is the preferred choice of distributing the peaker arms and it does preserve symmetry about the $z$ axis.

TABLE 1. Initial value of v and $\Delta$ v for various values of peakers $N_p$.

| $N_p$ | $\Delta v = \frac{2\pi}{N_p}$ *radians* | $v_1 = \begin{cases} 0.000\,\pi \text{ for } N_p \text{ odd} \\ \pi/N_p \text{ for } N_p \text{ even} \end{cases}$ |
|---|---|---|
| 1 | 2.000 $\pi$ | 0.000 $\pi$ |
| 2 | 1.000 $\pi$ | 0.500 $\pi$ |
| 3 | 0.667 $\pi$ | 0.000 $\pi$ |
| 4 | 0.500 $\pi$ | 0.250 $\pi$ |
| 5 | 0.400 $\pi$ | 0.000 $\pi$ |
| 6 | 0.333 $\pi$ | 0.167 $\pi$ |
| 7 | 0.286 $\pi$ | 0.000 $\pi$ |
| 8 | 0.250 $\pi$ | 0.125 $\pi$ |
| 9 | 0.222 $\pi$ | 0.000 $\pi$ |
| 10 | 0.200 $\pi$ | 0.100 $\pi$ |

The results of the numerical computations are shown in tabular (tables 2-6) as well as graphical (figures 15-19) forms. These distributions of peaker arms are optimal in the sense that the various peakers will then carry approximately equal currents.

TABLE 2. Computation of $\theta_i$ for $N_p = 1$ to 10 ; $\theta_o = 10°$

| $N_p$ | $\theta°_1$ | $\theta°_2$ | $\theta°_3$ | $\theta°_4$ | $\theta°_5$ | $\theta°_6$ | $\theta°_7$ | $\theta°_8$ | $\theta°_9$ | $\theta°_{10}$ |
|---|---|---|---|---|---|---|---|---|---|---|
| 1 | 0 | - | - | - | - | - | - | - | - | - |
| 2 | 10 | $-\theta_1$ | - | - | - | - | - | - | - | - |
| 3 | 0 | 17.23 | $-\theta_2$ | - | - | - | - | - | - | - |
| 4 | 4.15 | 23.85 | $-\theta_2$ | $-\theta_1$ | - | - | - | - | - | - |
| 5 | 0 | 7.27 | 30.14 | $-\theta_3$ | $-\theta_2$ | - | - | - | - | - |
| 6 | 2.69 | 10.01 | 36.23 | $-\theta_3$ | $-\theta_2$ | $-\theta_1$ | - | - | - | - |
| 7 | 0 | 4.82 | 12.52 | 41.94 | $-\theta_4$ | $-\theta_3$ | $-\theta_2$ | - | - | - |
| 8 | 1.99 | 6.69 | 14.92 | 47.48 | $-\theta_4$ | $-\theta_3$ | $-\theta_2$ | $-\theta_1$ | - | - |
| 9 | 0 | 3.64 | 8.39 | 17.23 | 52.77 | $-\theta_5$ | $-\theta_4$ | $-\theta_3$ | $-\theta_2$ | - |
| 10 | 1.59 | 5.10 | 10 | 19.48 | 57.83 | $-\theta_5$ | $-\theta_4$ | $-\theta_3$ | $-\theta_2$ | $-\theta_1$ |

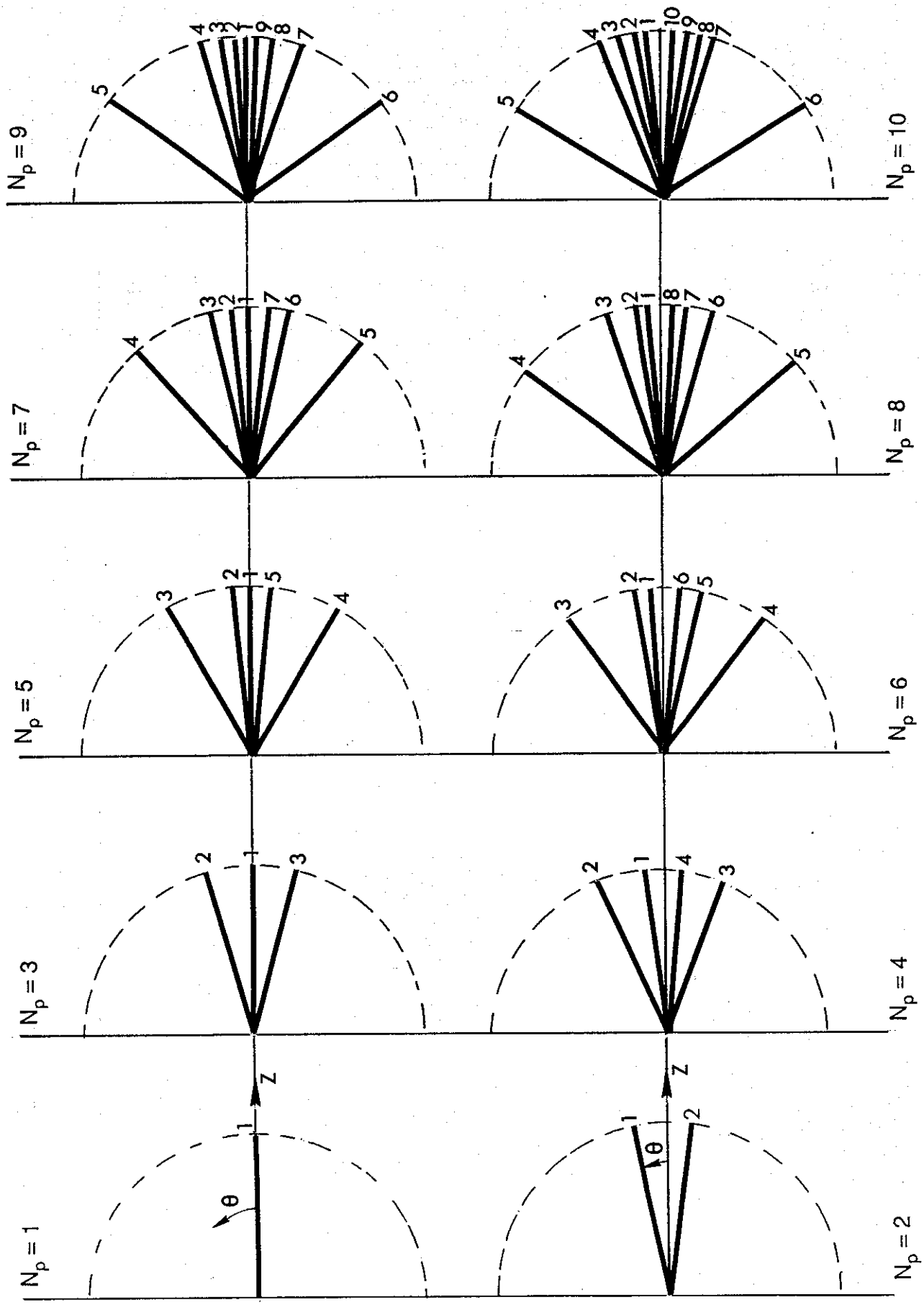


Figure 15. Peaker locations in ground plane $\theta_0 = 10°$.

TABLE 3. Computation of $\theta_i$ for $N_p = 1$ to 10 ; $\theta_o = 15°$

| $N_p$ | $\theta°_1$ | $\theta°_2$ | $\theta°_3$ | $\theta°_4$ | $\theta°_5$ | $\theta°_6$ | $\theta°_7$ | $\theta°_8$ | $\theta°_9$ | $\theta°_{10}$ |
|---|---|---|---|---|---|---|---|---|---|---|
| 1 | 0 | - | - | - | - | - | - | - | - | - |
| 2 | 15 | $-\theta_1$ | - | - | - | - | - | - | - | - |
| 3 | 0 | 25.69 | $-\theta_2$ | - | - | - | - | - | - | - |
| 4 | 6.24 | 35.26 | $-\theta_2$ | $-\theta_1$ | - | - | - | - | - | - |
| 5 | 0 | 10.92 | 44.11 | $-\theta_3$ | $-\theta_2$ | - | - | - | - | - |
| 6 | 4.05 | 15.01 | 52.24 | $-\theta_3$ | $-\theta_2$ | $-\theta_1$ | - | - | - | - |
| 7 | 0 | 7.25 | 18.75 | 59.95 | $-\theta_4$ | $-\theta_3$ | $-\theta_2$ | - | - | - |
| 8 | 3.00 | 10.05 | 22.29 | 66.99 | $-\theta_4$ | $-\theta_3$ | $-\theta_2$ | $-\theta_1$ | - | - |
| 9 | 0 | 5.48 | 12.60 | 25.69 | 73.49 | $-\theta_5$ | $-\theta_4$ | $-\theta_3$ | $-\theta_2$ | - |
| 10 | 2.38 | 7.67 | 15 | 28.97 | 79.46 | $-\theta_5$ | $-\theta_4$ | $-\theta_3$ | $-\theta_2$ | $-\theta_1$ |

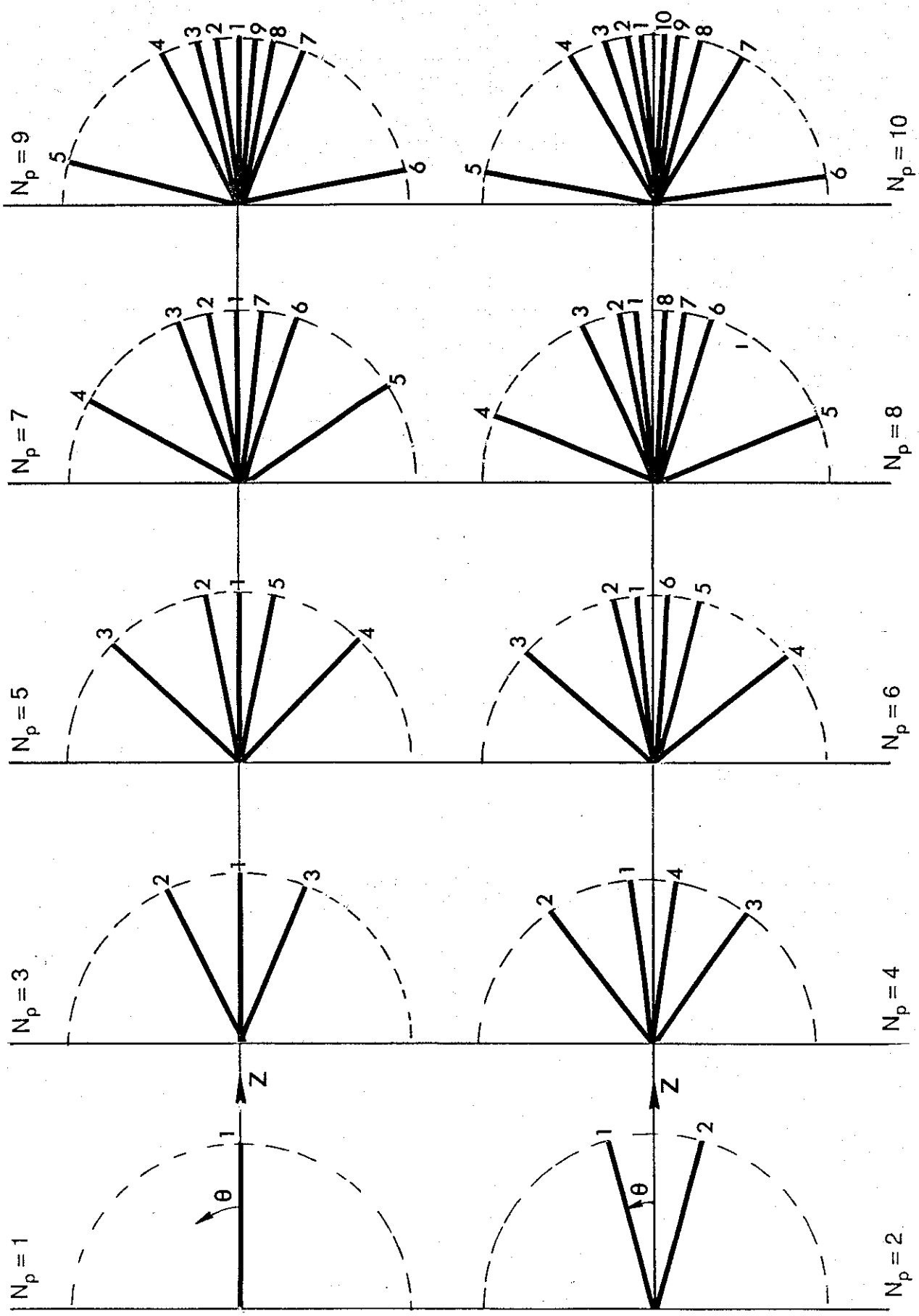


Figure 16. Peaker locations in ground plane $\theta_0 = 15°$.

TABLE 4. Computation of $\theta_i$ for $N_p = 1$ to 10 ; $\theta_o = 20°$

| $N_p$ | $\theta°_1$ | $\theta°_2$ | $\theta°_3$ | $\theta°_4$ | $\theta°_5$ | $\theta°_6$ | $\theta°_7$ | $\theta°_8$ | $\theta°_9$ | $\theta°_{10}$ |
|---|---|---|---|---|---|---|---|---|---|---|
| 1 | 0 | - | - | - | - | - | - | - | - | - |
| 2 | 20 | $-\theta_1$ | - | - | - | - | - | - | - | - |
| 3 | 0 | 33.96 | $-\theta_2$ | - | - | - | - | - | - | - |
| 4 | 8.35 | 46.12 | $-\theta_2$ | $-\theta_1$ | - | - | - | - | - | - |
| 5 | 0 | 14.60 | 56.97 | $-\theta_3$ | $-\theta_2$ | - | - | - | - | - |
| 6 | 5.42 | 20.02 | 66.80 | $-\theta_3$ | $-\theta_2$ | $-\theta_1$ | - | - | - | - |
| 7 | 0 | 9.70 | 24.93 | 75.37 | $-\theta_4$ | $-\theta_3$ | $-\theta_2$ | - | - | - |
| 8 | 4.02 | 13.44 | 29.57 | 83.11 | $-\theta_4$ | $-\theta_3$ | $-\theta_2$ | $-\theta_1$ | - | - |
| 9 | 0 | 7.34 | 16.83 | 33.96 | 90 | $-\theta_5$ | $-\theta_4$ | $-\theta_3$ | $-\theta_2$ | - |
| 10 | 3.20 | 10.27 | 20 | 38.18 | 96.14 | $-\theta_5$ | $-\theta_4$ | $-\theta_3$ | $-\theta_2$ | $-\theta_1$ |

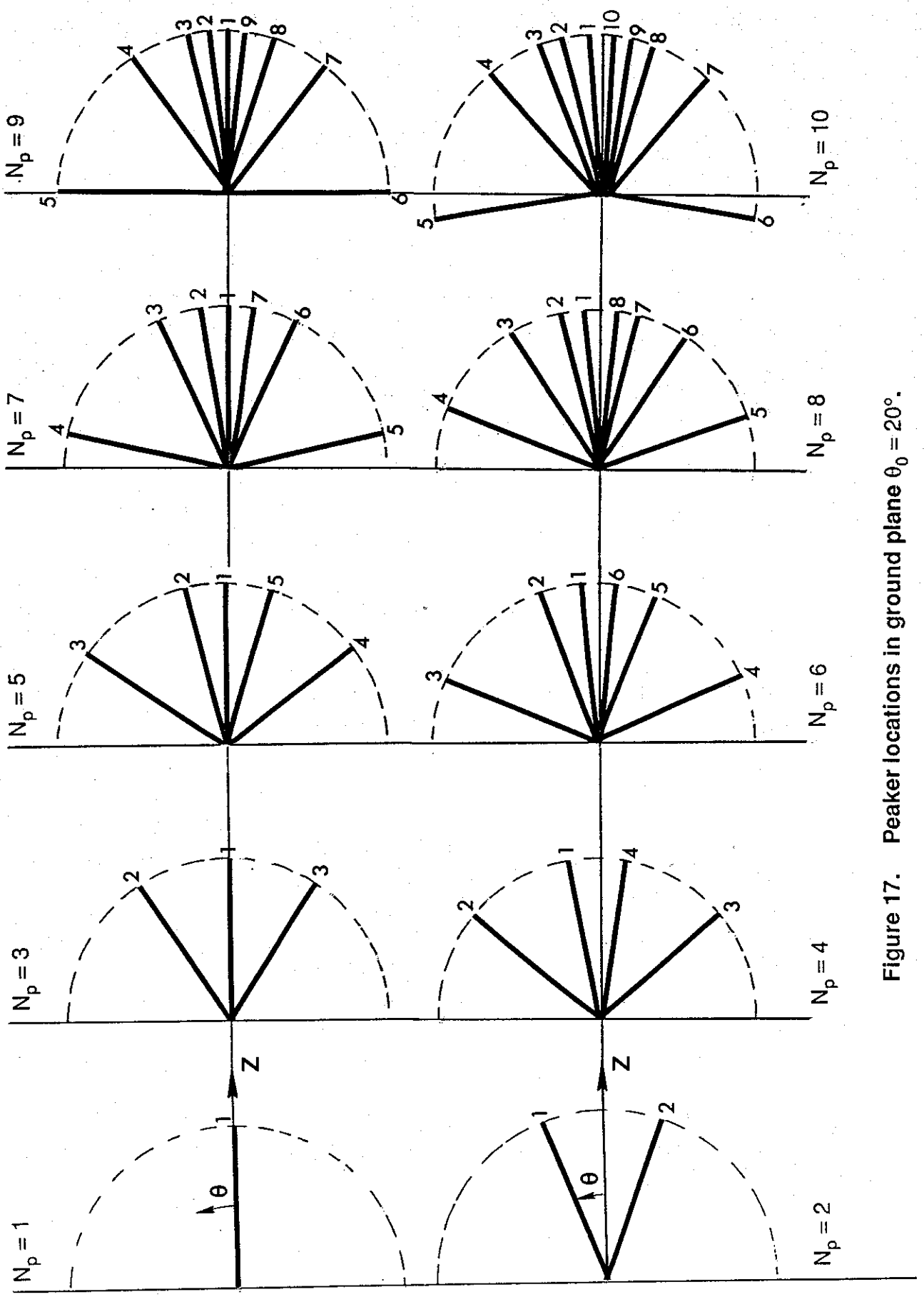


**Figure 17. Peaker locations in ground plane $\theta_0 = 20°$.**

TABLE 5. Computation of $\theta_i$ for $N_p = 1$ to 10 ; $\theta_o = 25°$

| $N_p$ | $\theta°_1$ | $\theta°_2$ | $\theta°_3$ | $\theta°_4$ | $\theta°_5$ | $\theta°_6$ | $\theta°_7$ | $\theta°_8$ | $\theta°_9$ | $\theta°_{10}$ |
|---|---|---|---|---|---|---|---|---|---|---|
| 1 | 0 | - | - | - | - | - | - | - | - | - |
| 2 | 25 | $-\theta_1$ | - | - | - | - | - | - | - | - |
| 3 | 0 | 42.01 | $-\theta_2$ | - | - | - | - | - | - | - |
| 4 | 10.49 | 56.31 | $-\theta_2$ | $-\theta_1$ | - | - | - | - | - | - |
| 5 | 0 | 18.30 | 68.61 | $-\theta_3$ | $-\theta_2$ | - | - | - | - | - |
| 6 | 6.81 | 25.02 | 79.32 | $-\theta_3$ | $-\theta_2$ | $-\theta_1$ | - | - | - | - |
| 7 | 0 | 12.18 | 31.07 | 88.33 | $-\theta_4$ | $-\theta_3$ | $-\theta_2$ | - | - | - |
| 8 | 5.05 | 16.85 | 36.71 | 96.2 | $-\theta_4$ | $-\theta_3$ | $-\theta_2$ | $-\theta_1$ | - | - |
| 9 | 0 | 9.22 | 21.07 | 42.01 | 103.00 | $-\theta_5$ | $-\theta_4$ | $-\theta_3$ | $-\theta_2$ | - |
| 10 | 4.02 | 12.89 | 25 | 47.02 | 108.91 | $-\theta_5$ | $-\theta_4$ | $-\theta_3$ | $-\theta_2$ | $-\theta_1$ |

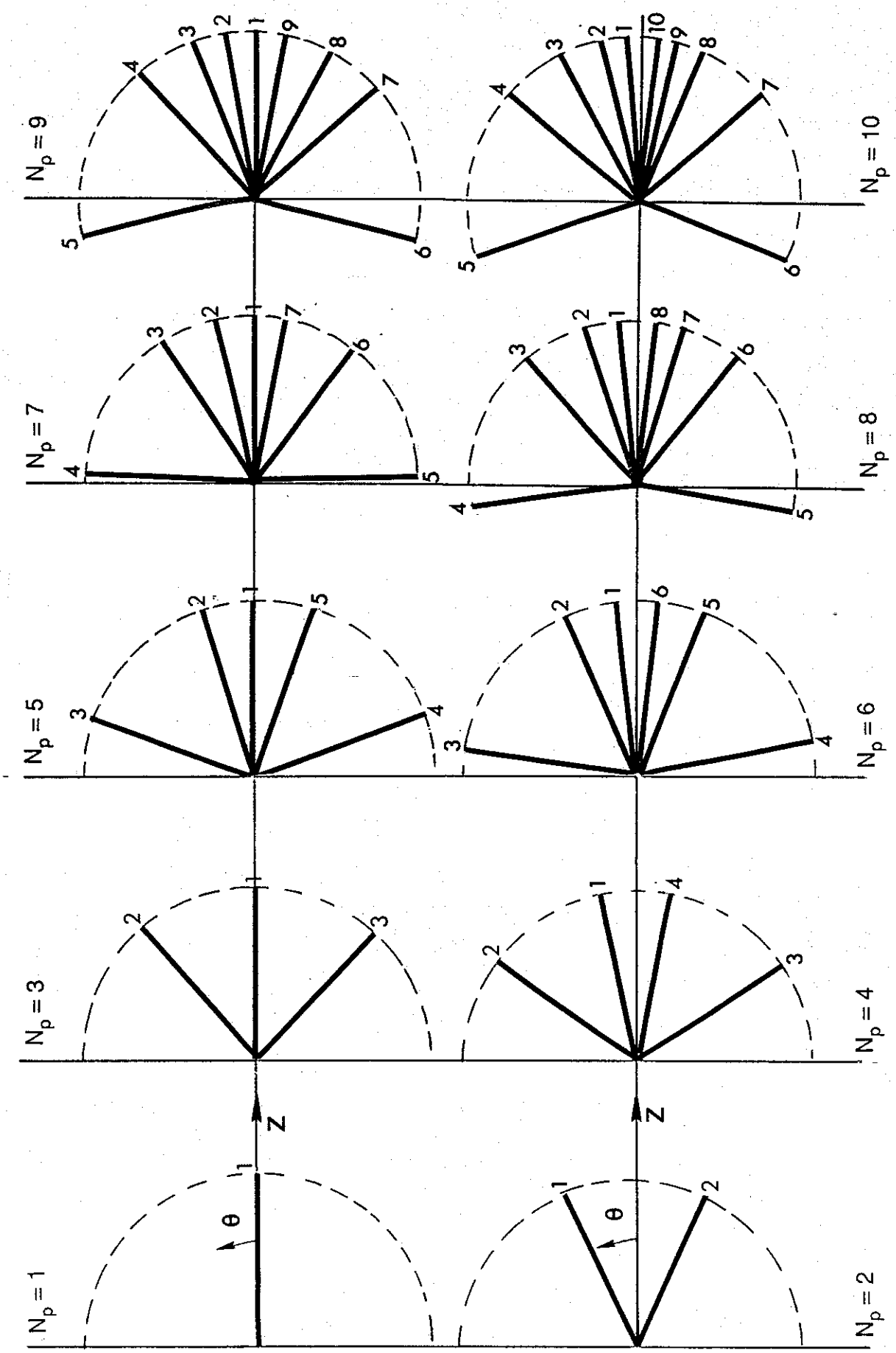


**Figure 18. Peker locations in ground plane $\theta_0 = 25°$.**

TABLE 6. Computation of $\theta_i$ for $N_p = 1$ to 10 ; $\theta_o = 30°$

| $N_p$ | $\theta°_1$ | $\theta°_2$ | $\theta°_3$ | $\theta°_4$ | $\theta°_5$ | $\theta°_6$ | $\theta°_7$ | $\theta°_8$ | $\theta°_9$ | $\theta°_{10}$ |
|---|---|---|---|---|---|---|---|---|---|---|
| 1 | 0 | - | - | - | - | - | - | - | - | - |
| 2 | 30 | $-\theta_1$ | - | - | - | - | - | - | - | - |
| 3 | 0 | 49.79 | $-\theta_2$ | - | - | - | - | - | - | - |
| 4 | 12.66 | 65.79 | $-\theta_2$ | $-\theta_1$ | - | - | - | - | - | - |
| 5 | 0 | 22.03 | 79.02 | $-\theta_3$ | $-\theta_2$ | - | - | - | - | - |
| 6 | 8.23 | 30.03 | 90.12 | $-\theta_3$ | $-\theta_2$ | $-\theta_1$ | - | - | - | - |
| 7 | 0 | 14.70 | 37.14 | 99.15 | $-\theta_4$ | $-\theta_3$ | $-\theta_2$ | - | - | - |
| 8 | 6.10 | 20.30 | 43.70 | 106.82 | $-\theta_4$ | $-\theta_3$ | $-\theta_2$ | $-\theta_1$ | - | - |
| 9 | 0 | 11.14 | 25.34 | 49.79 | 113.30 | $-\theta_5$ | $-\theta_4$ | $-\theta_3$ | $-\theta_2$ | - |
| 10 | 4.86 | 15.54 | 30 | 55.48 | 118.82 | $-\theta_5$ | $-\theta_4$ | $-\theta_3$ | $-\theta_2$ | $-\theta_1$ |

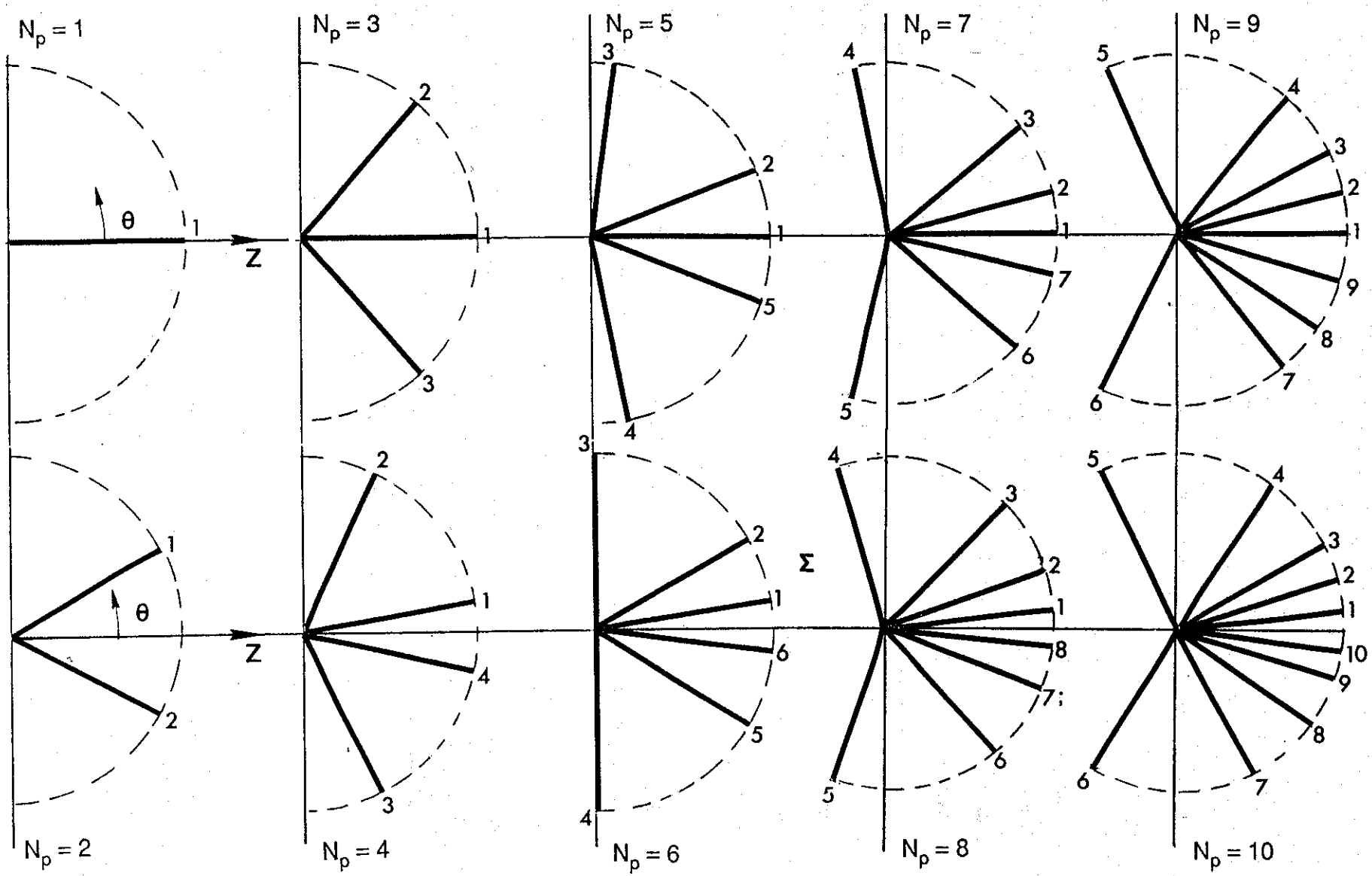


**Figure 19. Peaker locations in ground plane $\theta_0 = 30°$.**

## VI. Practical Considerations

There are several practical considerations in implementing the solution of optimal peaker locations in the ground plane. Firstly, the optimal locations derived in this note are for the situation where the return current is flowing through the ground plane in the discharge cycle of the pulser operation. On the other hand, it is highly desirable to ensure equal peaker currents during the charge cycle of the pulser as well. During the charge cycle, while charge transfer is taking place between Marx and the peakers, it certainly is desirable to avoid circulating or loop currents in peakers, which may persist after the output switch closure, causing waveform distortion. To avoid this, the Marx column behind the ground plane can be oriented at the same angle as the input launch angle. If proper connection is made between the other end (away from the switch) of Marx and the ground plane, the same peaker locations would serve to carry equal peaker currents.

Secondly, it is observed that a finite number of peaker arms (i.e., conductors) are employed to carry the total return current in the ground plane, thus causing a perturbation in the local ground plane fields. As $N_p$ increases, this perturbation is decreasing. However, small corrections to the peaker locations can be made to account for the finiteness of the value of $N_p$. This correction is similar to the case of simulating a "plate" by a finite number of wires [10], with each wire being parallel to the direction of propagation of the wave on the transmission line. If the wires or conductors are of radius $r_c$ and they are spaced a distance $d$ apart and if the wires support a uniform electric field on one side and no field on the other side, then a correction $\Delta y$ of the wires to an equivalent electrical position as a conducting plane [10] is given by

$$\Delta y = -\frac{d}{\pi} \ln\left(\frac{d}{\pi r_c}\right) \tag{39}$$

The above expression is strictly valid under the following assumptions:

a) The planar wire grid extends to infinity on both sides

b) wire diameter ($2r_c$) is much less than the spacing, and

c) all the wires are at the same potential

[10] has also shown that if the wire grid supports equal and opposite uniform fields on both sides of the grid, the shift $\Delta y$ is simply twice what is given by (39).

Although, the above approximations are not strictly valid in the present case, if the peaker arm radius ($r_p$) is small compared to the separation between the adjacent peakers, the expression $\Delta y$ can still be used in estimating a correction in position for the peakers. The net effect of this correction is that the peaker arms are raised somewhat from the ground plane into the launch section as illustrated in figure 20. The shifts $\Delta y_i$ are unequal and are larger for the peakers that are farther away from the $z$ axis, simply because they are farther apart. The exact shifts may easily be calculated, once we know the actual physical dimensions of the peaker arms and the number $N_p$. This results in peaker arms connected from a guard ring near the switch apex and sloping upward as indicated in figure 16. More detailed and qualitative description of the peaker connections follow.

Yet another important practical consideration is the electrical connections at both ends of individual peaker arms. Recall that the peakers are located in the ground plane, much like the spokes in a wheel, the wheel being a circular hole cut out in the ground plane. At the center is an output switch, typically a monocone with its apex coincident with the center of the peaker circle. The peakers connect to a circular guard ring around the center. At the other end, the peakers can have "teeth"-like metallic structures connecting to the ground plane. These are schematically depicted in figure 21. Referring to this figure, $r_g$, $r_p$ and $r_h$ are respectively the radii of the guard ring, peaker circle and the hole in the ground plane, with $(r_p - r_g)$ being the length of individual peaker arms. The radius of the hole in the ground plane $r_h$ is somewhat larger than $r_p$ in order to accommodate the "teeth"-like structures. These teeth aid in collecting and guiding the return current flow in the ground plane. In other words, they provide a smooth transition between the current carried by planar ground plane and the cylindrical conductors (i.e.,

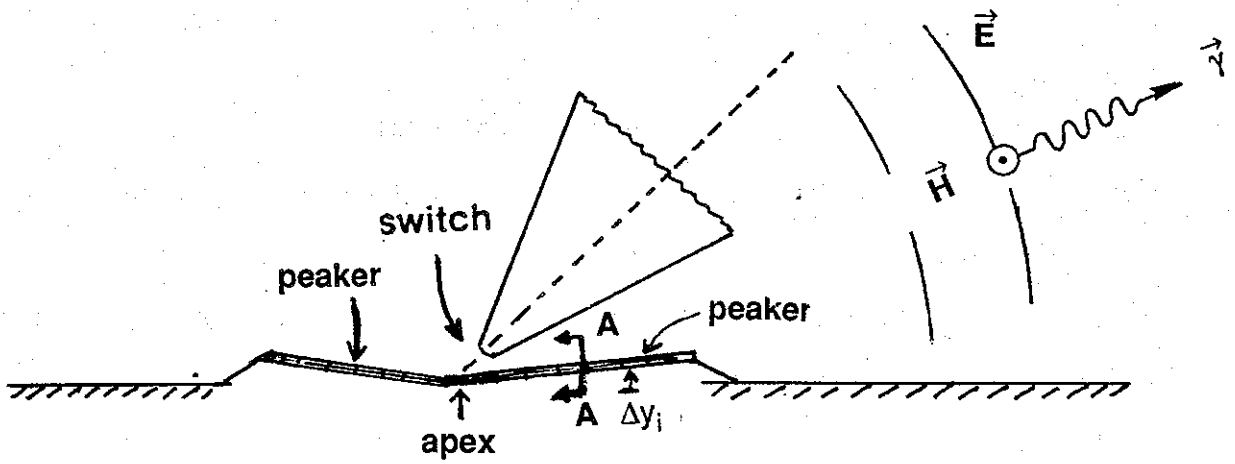


a) Side view

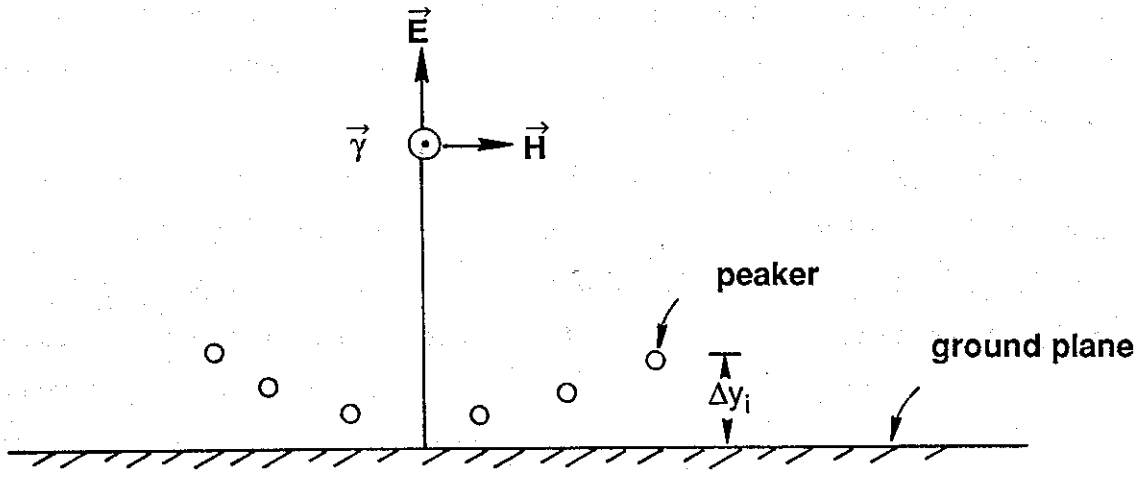


b) Cross sectional view at AA.

Figure 20. Two views of peaker lay out in the ground plane showing their elevated positions from the ground plane.

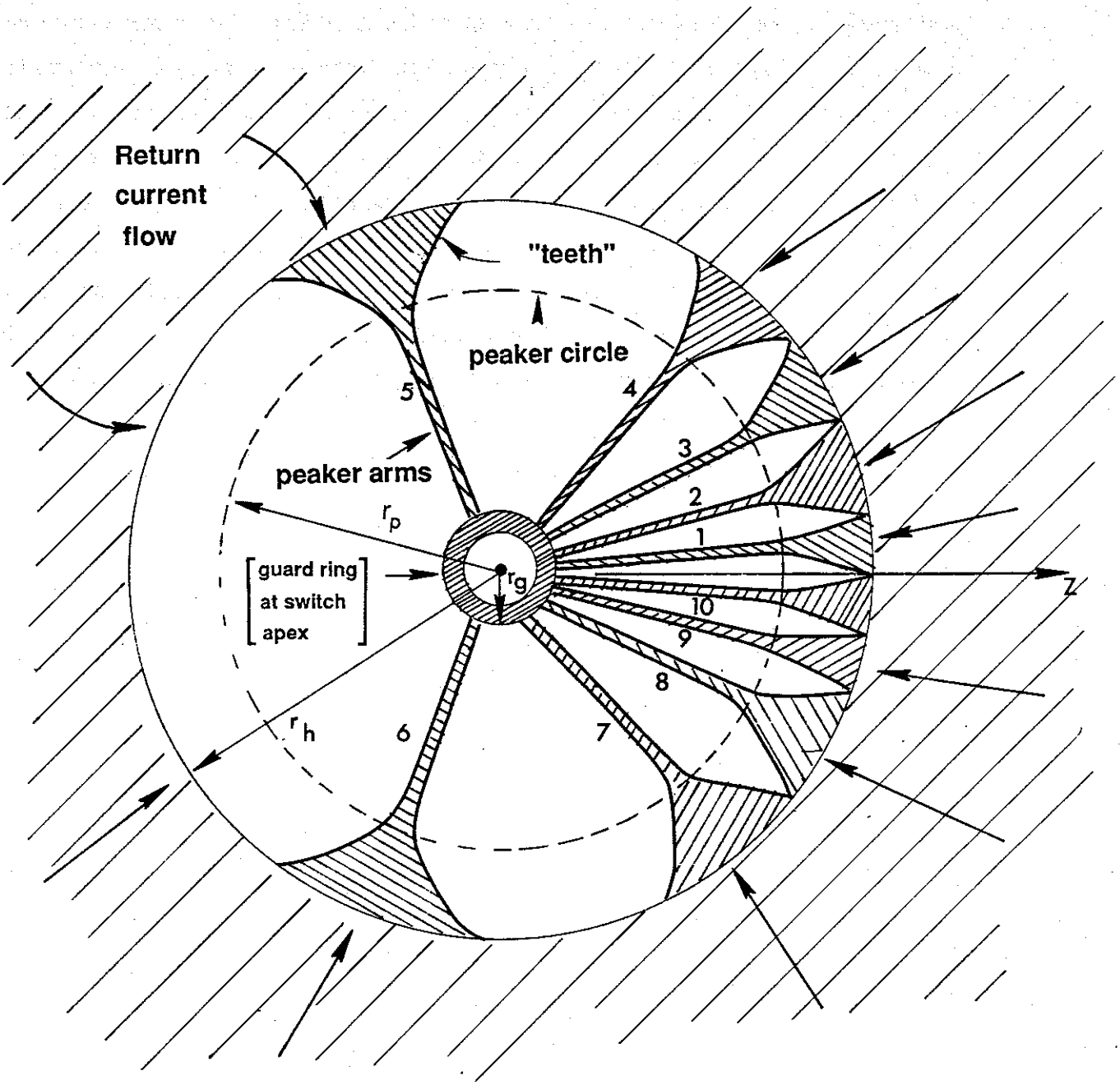


**Figure 21.** Suggested way of connecting the peaker arms (e.g., $\theta_0 = 25°$, $N_p = 10$).

peaker arms). The use of teeth at the end of peaker arms impacts to some extent, the choice of the value of $N_p$. On one hand, it is desirable to have as many peaker arms as possible so that individual peaker current $I_p$ is reduced and that the amount of metal removed from the ground plane is minimized. Having a large value for $N_p$ minimizes the field distortions in the vicinity of the apex. On the other hand use of peaker teeth may introduce a lower limit on the value of $N_p$ so that the size of the teeth does not become unwieldy. Some amount of experimental optimization of the number and distribution of peaker arms, size and shape of teeth is desirable. Such experiments could even be performed on low-voltage mock-up models of existing or planned pulse power systems.

## VII. Summary

In this note we have addressed the problem of determining an electromagnetically optimal way of distributing peaking-capacitor arms in the ground plane. These peaker arms are part of a Marx type of pulser system used to energize certain types of EMP simulators. Previous pulser configurations have employed the Marx column parallel to the ground plane. Optimal peaker locations around the Marx column have been worked out in the past. An alternate pulser configuration is one in which the Marx column is behind the ground plane, sloping at the same angle as the top plate. In such an alternate configuration, the peaker arms are then distributed in the ground plane and the output switch is located on the wave propagating side. The optimal peaker locations in the ground plane derived in this note ensure equal peaker currents during the discharge cycle when the return current flows in the ground plane. The formulation in this note helps in determining the locations of a given number $N_p$ of peaker arms. It uses a combination of stereographic projections and conformal mapping methods, basically to determine the current flow in the ground plane. Then one can distribute $N_p$ peakers in such a way that they all carry equal currents. The situation is one of replacing a circular conducting plane by a finite number of conductors. Consequently, certain corrections to peaker locations are possible resulting in the peaker arms being distributed slightly above the ground plane.

Furthermore, some practical considerations such as how best to connect the peaker arms to the switch electrode at the center and to the ground plane are discussed qualitatively. Certain experimental optimizations with low-voltage models appear to be in order.

The optimal peaker distributions are determined for illustrative purposes for five different input wave launching angles and ten values of $N_p$ for each launch angle. The results are presented in tabular as well as graphical forms. Calculations such as these can easily be performed for any specific launcher angle and $N_p$ value, to upgrade existing facilities or aid in the design of future facilities.

**References**


1. C.E. Baum, "EMP Simulators for Various Types of EMP Environments: An Interim Categorization," Sensor and Simulation Note 240, January 1978 and Joint Special Issue on the Nuclear Electromagnetic Pulse, IEEE Transactions on Antennas and Propagation, January 1978, pp. 35-53, and IEEE Transactions on Electromagnetic Compatibility, February 1978, pp. 35-53.

2. D.V. Giri, T.K. Liu, F.M. Tesche and R.W.P. King, Parallel Plate Transmission Line Type of EMP Simulators: A Systematic Review and Recommendations," Sensor and Simulation Note 261, 1 April 1980.

3. D.V. Giri and C.E. Baum, "Theoretical Considerations for Optimal Positioning of Peaking Capacitor Arms About a Marx Generator Parallel to a Ground Plan," Circuit and Electromagnetic System Design Note 33, 26 June 1985.

4. W.R. Smythe, Static and Dynamic Electricity, 3rd edition, McGraw-Hill, 1968.

5. C.E. Baum, "The Conical Transmission Line as a Wave Launcher and Terminator for a Cylindrical Transmission Line," Sensor and Simulation Note 31, 16 January 1967.

6. F.C. Yang and K.S.H. Lee, "Impedance of a Two-Conical-Plate Transmission Line," Sensor and Simulation Note 221, November 1976.

7. F.C. Yang and L. Marin, "Field Distributions on a Two-Conical-Plate and a Curved Cylindrical-Plate Transmission Line," Sensor and Simulation Note 229, September 1977.

8. C.E. Baum, "Impedances and Field Distributions for Symmetrical Two-Wire and Four-Wire Transmission Line Simulators," Sensor and Simulation Note 27, 10 October 1966.

9. C.Zuffada and N. Engheta, "Common and Differential TEM Modes for Two Wires Above a Ground Plane," Sensor and Simulation Note 305, July 1987.

10. C.E. Baum, "Impedances and Field Distributions for Parallel Plate Transmission Line Simulators," Sensor and Simulation Note 21, 6 June 1966.